Electromechanical coupling properties of [001], [011] and [111] poled $Pb(Mg_{1/3}Nb_{2/3})O_3$-0.32$PbTiO_3$ single crystals

Q. WAN*, C. CHEN, Y. P. SHEN
The State Key Laboratory, School of Astronautics and Aeronautics, Xi'an Jiaotong University, Xi'an, 710049, People's Republic of China
E-mail: wanqiang@mailst.xjtu.edu.cn; CChen@mail.xjtu.edu.cn

Published online: 28 March 2006

The electric field induced "butterfly" curves and polarization loops, and the stress induced strain and polarization responses of [001], [011] and [111] oriented $Pb(Mg_{1/3}Nb_{2/3})O_3$-0.32$PbTiO_3$ (PMN-0.32 PT) relaxor ferroelectric single crystals have been systematically investigated by experiment study. The focus is on the effect of constant compressive bias stress on the electromechanical coupling behavior along three crystallographic directions of PMN-0.32 PT single crystals. Dependence of the coercive field, remnant polarization, dielectric constant, and piezoelectric coefficient on the bias stress has been quantified for PMN-0.32 PT single crystals oriented in three different directions. Obtained results show that the large piezoelectric responses under zero compressive stress in [001] and [011] orientation are dominated by intrinsic crystal lattice while the engineered domain structure has a relatively minor effect. It is found that observed responses under stress cycle for [001] oriented crystals are due to polarization rotation and phase transformations. However, those for [011] and [111] oriented crystals are due to domain switching. The "butterfly" curves and polarization loops driven by electric field under different bias compression are described by two non-180° domain switching.

1. Introduction

The attractive piezoelectric properties of relaxor ferroelectric single crystals $Pb(Zn_{1/3}Nb_{2/3})O_3$-$x$$PbTiO_3$ (PZN-xPT) and $Pb(Mg_{1/3}Nb_{2/3})O_3$-$x$$PbTiO_3$ (PMN-xPT) have been extensively studied in recent years [1–3]. Compared to polycrystalline ferroelectric ceramics such as $Pb(Zr_{1/2}Ti_{1/2})$-O_3 (PZT), these materials exhibit greatly enhanced longitudinal piezoelectric coefficient (>2000 pC/N) and electrically induced strain (>1.7%) in the crystal directions which are inclined by certain angles to the spontaneous polarization direction [4–6]. PZN-xPT and PMN-xPT with outstanding properties are usually near the morphotropic phase boundary (MPB) [4, 7–8], which is in general located within a range of $x = 0.275$–0.33 for PMN-xPT [9, 10]. Various mechanisms have been proposed to explain the high performance of PZN-xPT and PMN-xPT along certain axes, e.g., the engineered domain structure (i.e., the multi-domain structure created by poling a crystal along a non-polar direction) [4, 11], the field induced polarization rotation and phase transformation [7, 12], the effects related to the proximity of a phase transition temperature [13, 14], and the crystal lattice property effect [15–17]. Notice that the comparable enhancement of piezoelectric properties along the same non-polar direction in mono-domain crystals and in crystals with engineered multi-domain structure indicates that the dominant contribution to the promising piezoelectric properties of ferroelectric single crystals could be the intrinsic lattice effects (i.e., crystal anisotropy) [15–17]. Owing to the superior electromechanical properties of ferroelectric single crystals, applications of them in micro-actuators, sensors, memories, and sonar seem certain to surge [3]. However, these devices usually experience complex coupling environment in practical applications (e.g. large temperature variation, high electric field and high stress). A mature level understanding of their responses to electrical, mechanical and temperature loading condition in different crystals directions are thus essential to fulfill the applications of these crystals.

*Author to whom all correspondence should be addressed.
0022-2461
DOI: 10.1007/s10853-006-6766-6

Rhombohedral phase of PZN-xPT($0<x<0.1$) and PMN-xPT($0<x<0.35$) exhibit excellent electromechanical properties along [001] and [110] orientations compared to the [111] (cubic cell reference) spontaneous polarization direction [4, 25]. A number of studies have focused on the loading induced behavior of [001], [011] and [111] oriented PZN-xPT and PMN-xPT single crystals [4, 8, 19, 25–29]. It has been shown that loadings in the form of electric field [4–12, 18–25] and stress [31–35] can lead to polarization rotation and phase transition, which change the crystal phase and domain structure of these single crystals, and hence dramatically alter their electromechanical properties. When an electric field is applied along the [001] direction of PZN-PT, polarization rotation occurs from [111] towards [001] via either M_A or M_B, depending the composition (e.g., the rotation is R-M_A-T for PMN-4.5 PT) [19, 42]. For [110]-oriented PMN-PT, polarization rotates from [111] to [110] via M_B when electric field is along [110] and ends up with an orthorhombic phase when the electric field exceeds a critical value. These single crystals can be polarized into a single domain state with [111] oriented electric field. Most available studies on the effect of bias stress on the crystal behavior focus only on uni-polar electric field loading (e.g., [12, 31–35]). However, it has been shown that the uni-polar and bi-polar responses of these crystals can be very different [31, 33, 34].

In this study, electric field induced "butterfly" curves and polarization loops for a set of compressive bias stress of [001], [011] and [111] poled PMN-0.32 PT single crystals will be explored by systematical experiment study. The effects of the compressive bias stress on the material properties along these three crystallographic directions of PMN-0.32 PT single crystals will be quantified. The underlying mechanisms for the observed feature will be explained in terms of phase transformation or domain switching, depending on the crystallographic direction.

2. Experimental methodology

At the test room temperature, PMN-0.32 PT single crystals used in this study are of morphotropic composition, and in the rhombohedral phase, very close to MPB. The pseudo-cubic [001], [011] and [111] directions of these crystals are determined by x-ray diffraction (XRD). Pellet-like specimens of dimensions $5 \times 5 \times 3$ mm^3 are then cut from these crystals, with the normal of the 5×5 mm^2 major specimen surfaces along the pseudo-cubic [001], [011] or [111] direction. All specimens are electroded with silver on the 5×5 mm major surfaces and poled along the [001], [011] and [111] orientations (i.e., the specimen thickness direction) under a field of 1.5 kV/mm. Note that there are eight possible dipole orientations along the body diagonal directions of unpoled PMN-0.32 PT single crystals (i.e., the ⟨111⟩ direction). When an electric poling field is applied to the crystals along the [001] direction, a multi-domain structure can be produced, comprising four degenerate states. For [011] direction poled single crystals, the number of degenerate states is two. The single crystals can be poled into a single domain state when they are poled along the [111] direction. The states of [001], [011] and [111] poled PMN-0.32 PT single crystals are sketched in Fig. 1, where solid arrows refer to the domain states induced by poling (also labeled as type 1 in Fig. 1b and c), dotted arrows represent possible domains switched from type 1 domains upon loading or unloading, and vice versa (also labeled as type 2).

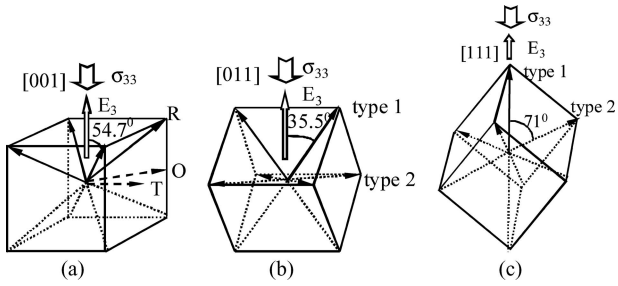

Figure 1 Sketches of possible domain states in (a) [001], (b) [011] and (c) [111] poled PMN-PT single crystals. The small rhombohedral distortion is neglected and all numbers and notations refer to a quasi-cubic unit cell.

Since the focus of this study is to explore the effect of bias stress on the electromechanical properties of PMN-0.32 PT single crystals along different crystallographic directions, experimental setup is adapted from Ref. [38] to allow simultaneously imposing uniaxial stress and electric field to the specimen along the thickness direction. Mechanical load is applied by a servo-hydraulic materials test system (MTS) and electric field is applied to the specimen using a high voltage power amplifier. Once the specimen is placed in the fixture, a compressive bias stress with magnitude of at least 0.4 MPa is maintained throughout the test to ensure electrical contact. Stress controlled loading instead of displacement controlled loading is adopted during the test, so that the specimen is not clamped but is free to move longitudinally when electric field E_3 and mechanical stress σ_{33} loading are applied, where subscript 3 refers to the thickness direction of the samples, corresponding to the [001], [011] and [111] direction of [001], [011] and [111] oriented PMN-0.32 PT single crystals, respectively. During test, polarization P_3 (or electric displacement) is measured using a modified Sawyer-Tower bridge, and the deformation (i.e., the strain) is monitored by two pairs of strain gauges (in total four strain gauges used) mounted on the four 5×3 mm^2 surfaces: one pair placed on two opposite 5×3 mm^2 surfaces is applied to measure the longitudinal normal strain ε_{33} along the [001], [011] and [111] direction and another pair to measure the transverse normal strain ε_{11} in the direction perpendicular to the [001], [011] and [111] direction respectively. Output of the strain gauges during deformation is recorded by a computer through a multiple-channel analog-to-digital (AD) converter.

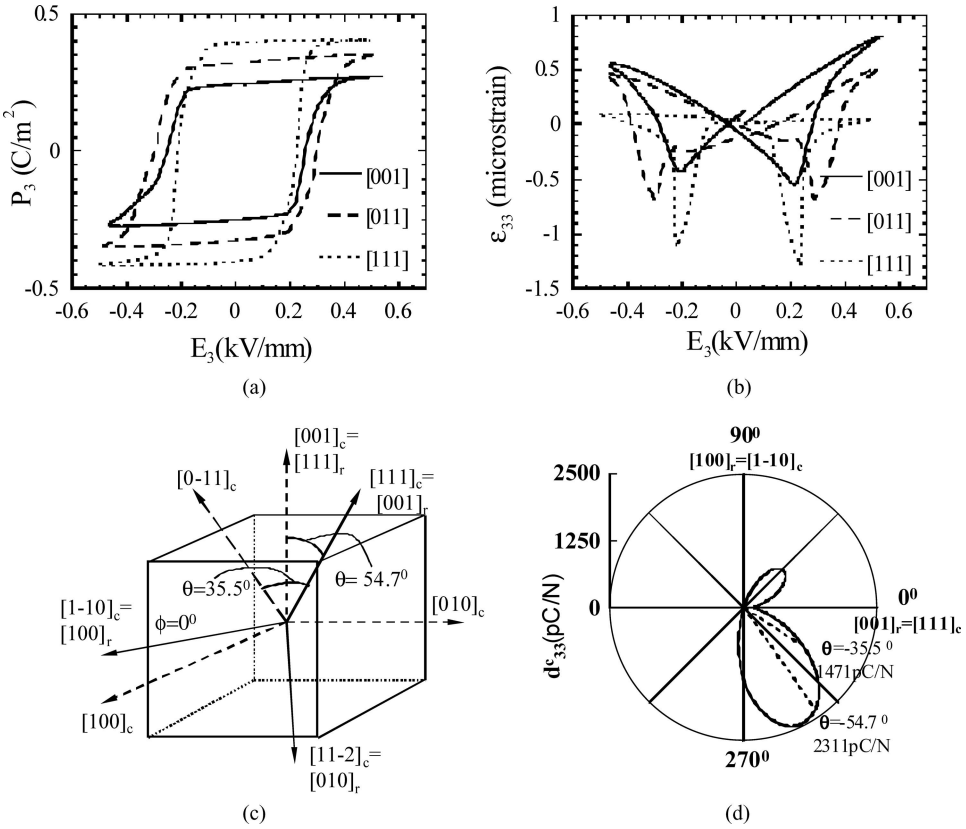

Figure 2 Electric field induced polarization and strain responses for [001], [011] and [111]-oriented crystals of PMN-0.32 PT: (a) $P_3 - E_3$ curves and (b) $\varepsilon_{33} - E_3$ curves. (c) Relationship between rhombohedral (solid lines) and cubic (dashed lines) coordinate systems. Subscripts r and c denote directions with respect to the rhombohedral and cubic coordinate systems, respectively. (d) Orientational dependence of piezoelectric coefficient d^*_{33} of PMN-0.32 PT in the polar plane.

The first set of tests is performed for electric field loading of triangular wave form of magnitude 0.5 kV/mm and frequency 0.02 Hz, free of stress loading. The low frequency is chosen to mimic quasistatic electric loading, which is of particular interest in this study [39]. Unless stated otherwise, this loading frequency for the electric field is used throughout the following test. The second set of tests consists of mechanical loading upon short circuited samples. The samples are compressed to -40 MPa and unloaded to -0.4 MPa at loading and unloading rate of 5 MPa/min, followed by an electric field which is sufficiently large to remove the residual stress and strain to re-polarize the samples. In the third set of tests, triangular wave form electric field is applied to the samples which are simultaneously subject to co-axial constant compressive stress preload. The magnitude of the preload is varied from test to test and is in the range between 0 and -40 MPa. Note that there is a time-dependent effect of the depolarization and strain responses under constant compressive stress [40]. To minimize this effect, each electric field loading starts after a holding time of 150 sec for a new stress preloading. It is found that three cycles of electric field loading and unloading are sufficient to produce stabilized response for each constant prestress, and the results for the last cycle are reported in the following.

3. Results and discussion

3.1. Crystallographic dependence of electric behavior and piezoelectric properties

The measured electric field induced polarization hysteresis loops and butterfly curves for [001], [011] and [111] oriented poled PMN-0.32 PT single crystals without stress loading are shown in Fig. 2a and b. The remnant polarizations P_r (defined as the polarization value at zero electric field), the coercive electric fields E_c (defined as the electric field value at zero polarization) and the piezoelectric coefficients d_{33} (defined as $d_{33} = \Delta\varepsilon_{33}/\Delta E_3$ where ΔE_3 is limited between -0.05 and $+0.05$ kV/mm, namely the slops of the $\varepsilon_{33} - E_3$ curves as the electric field passes through zero) depend strongly on the crystallographic orientation. From Figs 2a and b, one can calculate that $P_{r[001]}, P_{r[011]}$ and $P_{r[111]}$ are 0.247, 0.324 and 0.395 C/m^2, $E_{c[001]}$, $E_{c[011]}$ and $E_{c[111]}$ are 0.255, 0.298 and 0.216 kV/mm, and $d_{33[001]}$, $d_{33[011]}$ and $d_{33[111]}$ are 1828, 1049 and 200 pC/N, respectively. It is noticed that there are eight possible polarization orientations along the pseudo-cubic [111] for un-poled rhombohedral PMN-0.32 PT single crystals. Upon poling, the dipoles switch as close as possible to the applied electric field direction: For [001] poled crystals, there are four equivalent polar vectors along the [111] orientation, with an inclined angle of -54.7° from the poling field (Fig. 1a);

For [011] poled crystals, there are two equivalent polar vectors along the [111] direction (labeled as type 1 in Fig. 1b); For [111] poled crystals, there is one polar vector along [111] (type 1 in Fig. 1c). According to the domain configurations in Fig. 1, the remnant polarizations $P_{r[001]}$ and $P_{r[011]}$ are approximately related to $P_{r[111]}$ by $P_{r[001]} = P_{r[111]}/\sqrt{3}$ and $P_{r[011]} = \sqrt{2}P_{r[111]}/\sqrt{3}$, respectively. By taking the measured value for $P_{r[111]}$ (0.395 C/m^2), $P_{r[001]}$ and $P_{r[011]}$ are predicted to be 0.228 and 0.322 C/m^2, respectively, which are very close to the measured ones ($P_{r[001]} = 0.227$ C/m^2 and $P_{r[011]} = 0.324$ C/m^2). Therefore, the measured results are consistent with the domain configurations shown in Fig. 1.

It is also seen from Figs 2a and 2b that the coercive field is lowest for the [111] oriented crystals, and becomes successively higher for [001] and [110] orientations. This is same to Ref. [25] except for [110] orientation. This trend of coercive field is due to two reasons: One is due to reorientation driving force being proportional to the component of electric field aligned with the rhombohedral direction; The other one is due to the domain switching process. In [111]-oriented PMN-0.32 PT single crystals, there are two types of domains (shown as type 1 and type 2 in Fig. 1c). When the electric field is decreased from 0.5 kV/mm to −0.05 kV/mm, the strain first decreases linearly (see Fig. 2b). When the electric field is decreased further, the type 1 domain switches to type 2 domains, leading to abrupt displacement change. When the electric field exceeds the coercive field −0.216 kV/mm, the type 2 domains switch back to type 1 domain, recovering the deformation. In type 2 domain state, three equivalent polar vectors with an angle of 71° from the [111] direction can coexist and are separated by domain walls across which the normal components of electric displacement and displacement jump are zero. Ideally, this type of domain walls has no associated local stress or electric field. So the existing of type 2 domain state and the largest component of electric field along polarization direction induces the lowest coercive field in [111] orientation poled crystal. In the [011] orientation crystals, there are also two types of domains (i.e., type 1 and type 2 domain in Fig. 1b), the domain switching process is similar to [111]-poled crystals. In the type 2 domain state, however, the four possible polar vectors are perpendicular to the applied electric field (Fig. 1b). It is thus difficult to switch type 2 domain to type 1 domain only by applying electric field. Both the type 2 domain state and the smallest component of E contribute to the largest coercive field in [011] oriented crystals. In [001] oriented crystals, there will be no associated local stress or electric field, similar to type 2 domain state of [111] poled crystals. This feature again renders domain switching easy. On the other hand, the domain structure of [001] poled crystals is stable [4] and the component of electric field is smaller, giving the coercive field higher than that of [111] poled crystals but lower than that of [011] oriented crystals (see, Figs 2a and 2b).

Some researchers attribute the high piezoelectric coefficients along [001] and [011] oriented ferroelectric single crystals to the engineered domain state [4, 11]. It has also reported that, however, the piezoelectric coefficient along the [001] direction of single crystals with mono-domain structure is comparable to that of crystals with multi-domain structure [17], implying the origins of the high piezoelectric constants of PMN-0.32 PT single crystals may not be due to the engineered domain state. Instead, it could be due to the effect of crystal lattice properties. To further explore this issue, we follow Ref. [17] to calculate the piezoelectric coefficients d^*_{ij} along an arbitrary direction in a mono-domain crystal. For a direction defined by the Euler angles (ϕ, θ, ψ) (see Fig. 2c), d^*_{ij} is related to d_{ij} (measured along the principal crystallographic axes) by,

$$d^*_{33}(\phi,\theta) = d_{33}\cos^3\theta + (d_{15}+d_{31})\cos\theta\sin^2\theta - d_{22}\cos\phi\sin^3\theta(\cos^2\phi - 3\sin^2\phi) \quad (1)$$

With $d_{33} = 200$ pC/N taken from our measured value and $d_{15} = 4100$, $d_{31} = -90$ and $d_{22} = 1340$ pC/N from Ref. [41], $d^*_{33[111]}(0,\theta)$ for PMN–0.32 PT single crystals can be calculated and is shown in Fig. 3d. Note that in the case of $\phi = 0$ $\theta = -35.5°$ and $-54.7°$ correspond to [011] and [001] direction, respectively. $d^*_{33[011]} = 1471$ pC/N and $d^*_{33[001]} = 2311$ pC/N can be inferred from Figs 3d, which are not far away from our measured values ($d_{33[011]} = 1049$ pC/N and $d_{33[001]} = 1828$ pC/N). The small discrepancy between the predictions and measurements is believed to be due to the fact that the predictions are based on ideal mono-domain single crystals while the material parameters used in Eq. (1) are actually from less ideal mono-domain crystals (in fact, they are more or less multi-domain crystals). Nevertheless, we can conclude that the dominant contribution to the large [001] and [011] piezoelectric response should be the crystal anisotropy other than engineered domain state.

3.2. Crystallographic dependence of stress induced strain and polarization responses

Fig. 3 shows the measured $\sigma_{33} - \varepsilon_{33}$ and $\sigma_{33} - P_3$ curves for [001], [011] and [111] oriented short circuited samples. The results indicate obvious crystallographic anisotropy in stress inducing responses. From domain switching viewpoint, there should be no significant deformation in the thickness dimension of [001] poled crystal samples under stress loading, except for the elastic strain. However the longitudinal strain of [001] is contractive with a maximum magnitude of 0.3% under −40 MPa. The contractive strain of [001] oriented crystals is about twice as much as those of [011] (about −0.18%) and [111] (about −0.17%) oriented crystals under a loading of −40 MPa (Fig. 3a). This abnormal behavior of [001]-oriented crystals lies in that the mechanism underlying the stress

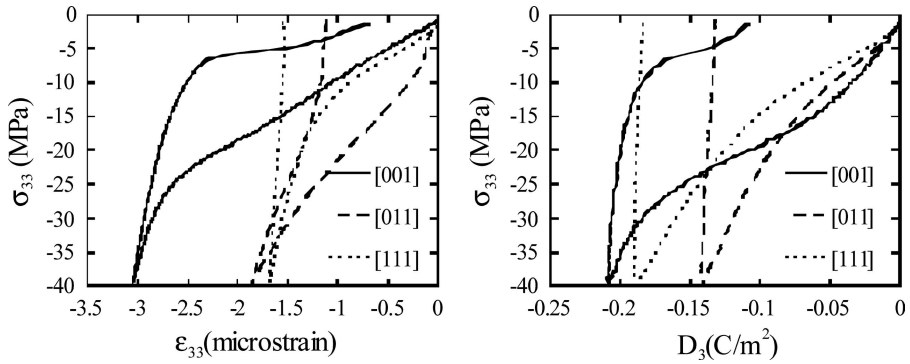

Figure 3 Compressive loading and unloading stress cycles induced polarization and strain responses for [001], [011] and [111]-oriented crystals of PMN-0.32 PT: (a) $\sigma_{33} - \varepsilon_{33}$ curves and (b) $\sigma_{33} - P_3$ curves.

induced response of [001]-oriented crystals is the R to O and T phase transition (see, Fig. 1a) rather than domain switching for [011] and [111] oriented crystals [42]: the lattice distortion due to phase transition induces large deformation in the thickness dimension of [001] poled crystals. In [011] and [111]-poled crystals, on the contrary, the type 2 multi-domain state induced by compressive stress is the stable and preferred state (Figs 1b and 1c), and can form more easily by domain switching than phase transformation. Therefore, the stress induced strain and polarization curves in [011] and [111] orientation crystals are similar to those of ferroelectric polycrystals of which domain switching is also the dominant deformation mechanism (Figs 3a and 3b). During the unloading of [001] oriented crystals (corresponding to the returning to R phase of the unstable O phase), the $\sigma_{33} - \varepsilon_{33}$ and $\sigma_{33} - P_3$ curves show obvious nonlinear behavior. Note that the remnant strain and polarization at the end of unloading are attributed to the stable T phase which does not switches back to the R phase. For [011] and [111]-oriented crystals, however, there is only domain switching (i.e., switching between type 1 and type 2 domains) and no phase transformation occurs. During unloading, the $\sigma_{33} - \varepsilon_{33}$ curves and $\sigma_{33} - P_3$ curves of [011] and [111] show linear response since almost no domain switches back (Figs 3a and 3b).

3.3. Crystallographic dependence of electric field induced behavior at constant bias compressive stress

The $\varepsilon_{33} - E_3$ "butterfly" curves and $P_3 - E_3$ hysteresis loops of [001], [011] and [111] poled crystals under different constant compressive bias stresses are shown in Fig. 4. Dependence of the electric coercive E_c, remnant polarization P_r, dielectric permittivity χ_{33}, piezoelectric coefficient d_{33} and aggregate strain $\Delta\varepsilon$ for [001], [011] and [111] oriented crystals on the compressive bias stress is summarized in Fig. 5. The aggregate strain $\Delta\varepsilon$ is defined as the difference between the maximum and minimum strain for a complete responsive butterfly curves. Similar to d_{33}, χ_{33} are calculated by $\Delta P_3/\Delta E_3$ where ΔP_3 is the polarization difference between -0.05 and $+0.05$ kV/mm. The calculated χ_{33} within such a small field range is almost equal to the slope of $P_3 - E_3$ hysteresis loops when the electric field passes through zero. The calculated χ_{33} includes both the reversible (intrinsic dielectric property) and irreversible (extrinsic domain switching and phase transformation related property) contributions of the material, which is generally higher than the permittivity measured by a dynamic method [32].

The influence of the preloaded compressive stress on the aggregate strain $\Delta\varepsilon$, remnant polarization P_r and piezoelectric coefficient d_{33} seems to be similar for [001], [011] and [111] oriented crystals: The remnant polarization P_r decreases with increasing the magnitude of the compressive prestress; The aggregate strain $\Delta\varepsilon$ and piezoelectric coefficient d_{33} first increase and then decrease with the magnitude of the prestress increasing. As suggested earlier, however, the underlying mechanisms for the electromechanical behavior of [001] [011], and [111] oriented crystals are different. The change of the dielectric permittivity χ_{33} [001] oriented crystals under compressive stress is similar to that of χ_{33} induced by temperature: near the phase transformation temperature there is a peak in the χ_{33} curves [43 , 44]. As is shown in Fig. 5c, there is a small peak near -6 MPa and a big peak near -20 MPa in χ_{33} curves for [001] oriented crystals. This may be due to R-M (near -6 MPa) and M-R and M-O phase transformation (near -20 MPa). On the other hand, there is no obvious peak in χ_{33} curves for [011] and [111]-oriented crystals (Fig. 5c). The change of χ_{33} curves induced by compressive stress and the aforementioned stress induced strain and polarization responses are consistent with the hypothesis that there is phase transformation for [001]-orientated crystals under compressive stress.

As suggested by Fu et al. [7], for [001] oriented crystal origins of large aggregate strain and high piezoelectric coefficient at a moderate compressive bias stress (i.e., around -20 MPa for the single crystals considered here) may be attributed to the stress induced intermediate states between rhombohedral and tetragonal phases. Under a bias stress of about -20 MPa, PMN-0.32 PT single crystals, after a phase transformation, are in a state of

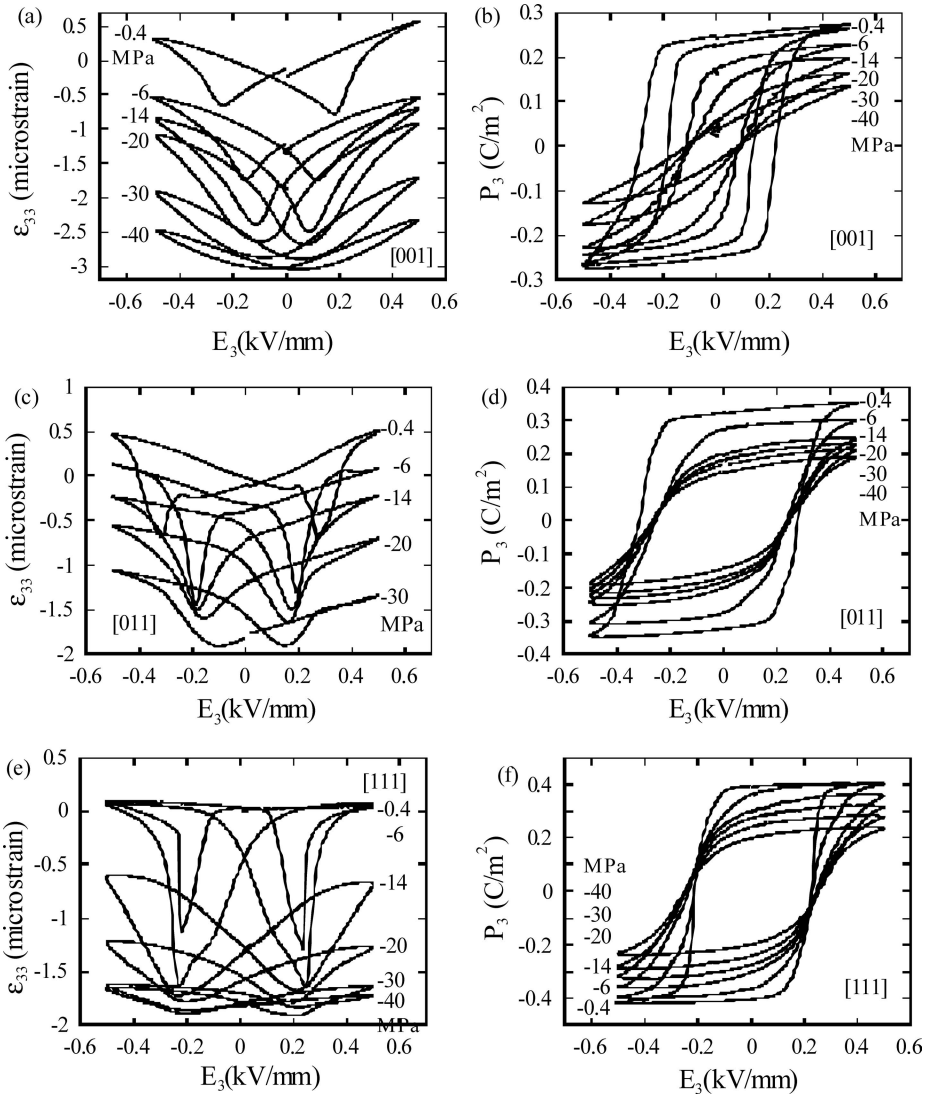

Figure 4 Electric field induced $\varepsilon_{33} - E_3$ and $P_3 - E_3$ curves at different compressive bias stresses: (a) and (b) for [001]-oriented; (c) and (d) for [011]-oriented, (e) and (f) for [111]-oriented.

monoclinic phase which has a larger c/a (c and a are lattice parameters) and a smaller polarization component along the field direction than those of rhombohedral phase [20], implying electric field induced greater aggregate strain and piezoelectric coefficient (Figs 5d and 5e). With the magnitude of the compressive bias stress increased further (i.e., $\sigma_{33} = -30$ and -40 MPa), the [001] oriented single crystals are in the state of a mixture of orthorhombic and tetragonal phases. Although O and T phases also have large c to a ratio, the presence of a large compression has an opposite effect (i.e., preventing larger deformation induced by electric field) and results in small aggregate strain (Fig. 5e).

As is noted, the polarization rotation introduced by compression gives rise to θ in $d^*_{33}(\phi, \theta)$ in the range between -54.7° and -90° (the angle between loading and polarization direction of T or O phase) under -20 MPa, and results in larger d^*_{33} in accordance with Eq. (1) (see in Fig. 5d). When the magnitude of the compressive bias stress increases further, θ approaches 90° and d^*_{33} becomes smaller. Meanwhile, the remnant polarization P_r and coercive field E_c decrease monotonically with the applied compressive bias stress because of the decreased component polarization along the [001] direction under compression (Fig. 5b).

Under zero stress, the initial state of [011]-oriented crystals is of multi-domain with two equivalent polarization directions (Fig. 1b). For [111]-oriented crystals, the initial state is of mono-domain with polarization direction in the [111] direction (Fig. 1c). When the applied electric field decreases from 0.5 kV/mm to $-E_c$, the strain and polarization decrease linearly. Upon approaching $-E_c$, domain state switches to four polar domain state for [011] oriented crystals (type 2 in Fig. 1b) and three polar domain state for [111] oriented crystals (type 2 in Fig. 1c), giving the jumps in strain and polarization responses. When electric field exceeds $-E_c$, domain complete second switching, from four polar domain state to two polar domain state for [011] oriented crystals and from three polar domain state to mono-domain state for [111] oriented

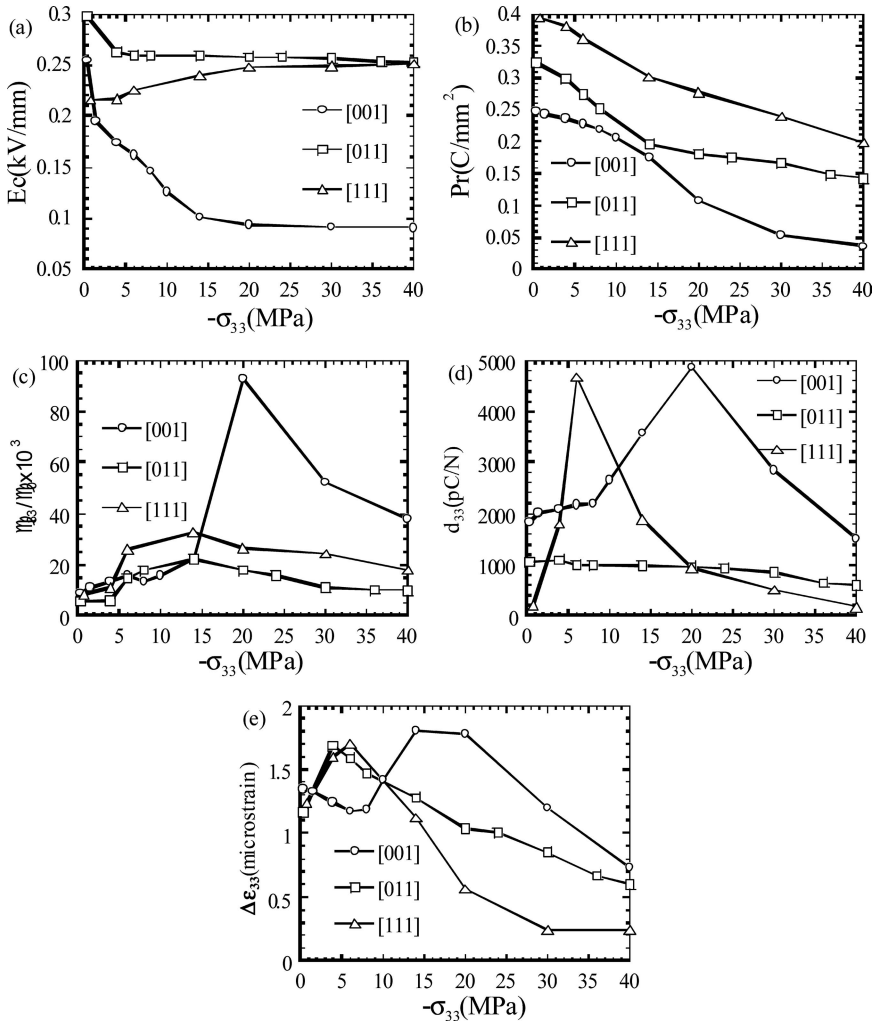

Figure 5 Effect of compressive bias stress on (a) the coercive field E_c, (b) remnant polarization P_r, (c) piezoelectric constant d_{33}, (d) relative dielectric constant χ_{33}/χ_0, and (e) and aggregate strain $\Delta\varepsilon_{33}$.

crystals. When the electric field reaches −0.5 kV/mm, the strain and polarization change linearly again (Fig. 5).

Note that compressive stress can induce domain switching in [011] and [111]-orientated crystals. When compressive stress is superimposed on the samples, the shapes of $\varepsilon_{33} - E_3$ and $P_3 - E_3$ curves are different from those under the zero stress state (Figs 4c–f). Due to compression inducing depolarization, the remnant polarization decreases in [011] and [111] oriented crystals (Fig. 5b). A low compressive stress (e.g., −5 MPa for [011], −7 MPa for [111]) can lead to type 1 to type 2 domain switching. As a result, more domains take part in switching during the electric field loading cycle and larger aggregate strain $\Delta\varepsilon$ than under zero compressive stress is observed. This partly explains the observed features in Fig. 5e.

4. Conclusions

Stress induced strain and polarization, and electric field induced "butterfly" curves and polarization loops for a set of compressive bias stress for [001], [011] and [111] poled PMN-0.32 PT single crystals are experimentally explored. Obtained results indicate that high piezoelectric responses of PMN-0.32 PT single crystals are controlled by the anisotropy of the crystals and the multi-domain structure (i.e., engineered domain structure) has a relatively minor effect. Analysis shows that in all three directions the electric field induced aggregate strain $\Delta\varepsilon$ and piezoelectric constant d_{33} increase with increasing the magnitude of the compressive bias stress. However, when the magnitude of the compressive bias stress is further increased the electric field induce $\Delta\varepsilon$ and d_{33} decrease. As a result, an optimized compressive bias stress exists for the purpose of enhancing the electromechanical properties of [001] and [111] oriented PMN-0.32 PT single crystals. These results have apparent importance in the design of actuators and sensors using PMN-0.32PT single crystals. It is found that the observed stress induced strain and polarization in [001]-oriented PMN-0.32 PT can be described by a polarization rotation mechanism, i.e., polarization rotates from rhombohedral (R) to orthohombic (O) and tetragonal (T) phases through the intermediate Monoclinic (M) phase during loading, and O to R transition during unloading.

However, domain switching is believed to be the main mechanism dictating the electromechanical behavior of [011] and [111] oriented PMN-0.32 PT single crystals.

Acknowledgments

The authors are grateful for the financial support by the Natural Science Foundation of China (No. 90205030, 10472088, 10425210) and the Ministry of Education of China.

References

1. B. NOHEDA, *Curr. Opin. Solid State Mater Sci.* **6** (2002) 27.
2. L. BELLAICHE, *Curr. Opin. Solid State Mater Sci.* **6** (2002) 19.
3. S. E. PARK and W. HACKENBERGER, *Curr. Opin. Solid State Mater Sci.* **6** (2002) 11.
4. S. E. PARK and T. R. SHROUT, *J. Appl. Phys.* **82** (1997) 1804.
5. R. F. SERVICE, *Science* **275** (1997) 1878.
6. D. VIEHLAND, A. AMIN and F. J. LI, *Appl. Phys. Lett.* **79** (2001) 1006.
7. H. FU and R. E. COHEN, *Nature (London)*, **403** (2000) 281.
8. S. W. CHOI, T. R. SHROUT, S. J. JANG and A. S. BHALLA, *Mater. Lett.* **8** (1989) 253.
9. Z. G. YE and M. DONG, *J. Appl. Phys.* **87** (2000) 2312.
10. S. W. CHOI and J. M. JUNG, *Ferroelectrics* **189** (1996) 27.
11. S. WADA, S. SUZUKI, T. NOMA, T. SUZUKI, M. OSADA, M. KAKIHANA, et al., *Jpn. J. Appl. Phys.* **38** (1999) 5505.
12. E. A. MCLAUGHIN, T. LIU and C. S. LYNCH, *Acta. Mater.* **52** (2004) 3849.
13. J. FITZGERALD, J. HUANG and J. SHORE, *Ferroelectrics* **233** (1999) 187.
14. G. A. SAMARA, E. L. VENTURINI and V. H. SCHMIDT, *Appl. Phys. Lett.* **76** (2000) 1327.
15. K. NAKAMURA, T. TOKIWA and Y. KAWAMURA, *J. Appl. Phys.* **91** (2002) 9272.
16. D. DAMJANOVIC, F. BREM and N. SETTER, *Appl. Phys. Lett.* **80** (2002) 652.
17. D. DAMJANOVIC, M. BUDIMIR, M. DAVIS and N. SETTER, *Appl. Phys. Lett.* **83** (2003) 527.
18. G. S. XU, H. S. LUO and H. Q. XU, *Phys. Rev. B.* **64** (2001) 020102.
19. D. VIEHLAND, J. F. LI and A. AMIN, *J. Appl. Phys.* **92** (2002) 3985.
20. B. NOHEDA, Z. ZHONG and D. E. COX, *Phys. Rev. B.* **65** (2002) 224101.
21. Z. G. YE, B. NOHEDA and M. DONG, *Phys. Rev. B.* **64** (2001) 184114.
22. L. BELLAICHE, A. GARCIA and D. VANDERBILT, *Phys. Rev. Lett.* **84** (2000) 5427.
23. L. BELLAICHE, A. GARCIA and D. VANDERBILT, *Phys. Rev. B.* **64** (2001) 060103.
24. Y. LU, D. Y. JEONG and Z. Y. CHENG, et al., *Appl. Phys. Lett.* **78** (2001) 3109.
25. T. LIU and C. S. LYNCH, *Acta. Mater.* **51** (2003) 407.
26. D. VIEHLAND and J. F. LI, *J. Appl. Phys.* **94** (2003) 7719.
27. J. CHRISTELLE, J. F. LI and D. VIEHLAND, *J. Appl. Phys.* **95** (2004) 5671.
28. D. VIEHLAND, J. F. LI, K. GITTINGS and A. AMIN, *J. Appl. Phys.* **83** (2003) 132.
29. H. CAO, B. FANG, H. XU and H. LUO, *Mater. Res. Bull.* **37** (2002) 2135.
30. C. S. TU, C. L. TSAI and V. H. SCHMIDT, et al., *J. Appl. Phys.* **89** (2001) 7908.
31. D. VIEHLAND, J. POWERS and L. EWART, et al., *J. Appl. Phys.* **88** (2000) 4907.
32. D. VIEHLAND and J. POWERS, *Appl. Phys. Lett.* **78** (2001) 3112.
33. D. VIEHLAND and J. POWERS, *J. Appl. Phys.* **89** (2001) 1820.
34. D. VIEHLAND, L. EWART and J. POWERS, et al., *J. Appl. Phys.* **90** (2001) 2479.
35. D. VIEHLAND, J. F. LI and E. MCLAUGHLIN, et al., *J. Appl. Phys.* **95** (2004) 1969.
36. N. NOBEA, D. COX and G. SHIRANE, et al., *Phys. Rev. Lett.* **86** (2001) 3891.
37. J. K. SHANG and X. TAN, *Acta. Mater.* **49** (2001) 2993.
38. J. SHIEH, J. E. HUBER and N. A. FLECK, *Acta. Mater.* **51** (2003) 6123.
39. Q. WAN, C. CHEN and Y. P. SHEN, *J. Mater. Sci.* (2005) in press.
40. D. MUNZ and T. FETT, Springer Series in Materials Science, Springer-Verlag, Berling, (1999) 167.
41. R. ZHANG, B. JIANG and W. CAO, *Appl. Phys. Lett.* **82** (2003) 787.
42. Q. WAN, C. CHEN and Y. P. SHEN, *J. Appl. Phys.* **98** (2005) 024103.
43. Z. L. YAN, X. YAO and L. Y. ZHANG, *Ceramics International* **30** (2004) 1423.
44. Y. P. GUO, H. S. LUO and H. Q. XU et al. *Ferroelectrics* **281** (2002) 79.
45. P. M. CHAPLYA and C. P. CARMAN, *J. Appl. Phys.* **90** (2001) 5278.

Received 11 May
and accepted 13 September 2005